Chapter 1
Smart Nanomaterials and Sensing Devices: An Introduction

Virendra Kumar, Vandana Nagal, Ajit Kumar, Ashwani Kumar Singh, Aurangzeb Khurram Hafiz, and Kedar Singh

Abstract Nanotechnology-adapted sensing technologies or sensing devices could detect environmental changes with the help of computer processors where signal can be readout. With the evolution in advancement of nanotechnology, it has sparked recently in the sensing field also and opened new windows for future engineered devices having great performance. To meet social demands, such as hazard chemical detection, pollution problems and environmental remediation, harmful energy detection, and biomedical treatments, etc., sensors plays an important role. The smart nanomaterials of different dimensions like 0D, 1D, and 2D improved device sensitivity. From smart nanomaterials, synthesis to device fabrication via well-known top-down technology in synergistic with bottom-up advances will allow nanostructures full exploitation at a sensor device scale. This trend of advancement in nanomaterials will continuously evolve sensing technology, and in turn, its impact on our daily life will be visible.

Keywords Nanomaterials · Quantum dots · Sensing · Devices · Gas sensor

1.1 Introduction

Energy storage, medical diagnostics, food technology, and sensor applications all use nanotechnologies and nanomaterials in nanoscale devices [1]. Nanomaterials are a novel class of materials with a wide range of fascinating applications in fields requiring light emission and absorption, including in vivo imaging, light-emitting

V. Kumar (✉) · A. Kumar · K. Singh
Nanotechnology Lab, School of Physical Sciences, Jawaharlal Nehru University (JNU), New Delhi 110067, India
e-mail: virend72_sps@jnu.ac.in

V. Nagal · A. K. Hafiz
Quantum and Nano-photonics Research Laboratory, Centre for Nanoscience and Nanotechnology, Jamia Millia Islamia (A Central University), New Delhi 110025, India

A. K. Singh
Department of Physics, Deshbandhu College, University of Delhi, Kalkaji, New Delhi 110019, India

R. K. Sonker et al. (eds.), *Smart Nanostructure Materials and Sensor Technology*,
https://doi.org/10.1007/978-981-19-2685-3_1

devices, photodetection, and solar energy conversion, to name a few [2]. Nanomaterials are used to design and develop novel optoelectronic devices (photonics devices) that improve performance while lowering costs [1]. A nanostructure can be classified as (1) 0D (quantum dots), (2) 1D (quantum wires, rods, belts, and tubes), or (3) 2D (thin films or quantum wells, for example) [3]. Monodisperse colloidal semiconductor nanocrystals (NCs) have been synthesised using the hot precursor injection approach since 1993. This method allows semiconductor particles to grow in solution, resulting in quantum restricted materials with an atom-like spectrum [4]. Because of their narrow, size-tunable emission spectra and broad absorption and excitation spectrum, monodisperse colloidal NCs are well suited for solution-based processing. These properties make visible-emitting NCs particularly interesting for lighting and display applications [2]. Because of the lower control and carrier mobilities associated with colloidal syntheses than those produced using conventional methods, the semiconductor world has been sceptical for a long time. Various methods, such as top-down approaches (e.g. electron beam lithography, reactive ion etching/or wet-chemical etching), or bottom approaches, can be used to synthesise NCs [4]. The NCs were synthesised using a variety of self-assembly strategies in the bottom-up approach, which can be roughly separated into wet-chemical and vapour-phase procedures. Microemulsion, sol–gel, competitive reaction chemistry, hot-solution decomposition (i.e. the aforementioned hot-injection approach), and electrochemistry are all considered wet-chemical processes. Vapour-phase approaches include self-assembly of nanostructures in material generated via molecular beam epitaxy (MBE), sputtering, liquid metal ion sources, and gaseous monomer aggregation [3]. As a result, significant improvement has been made in size, form, and composition management over the previous 30 years. More than half of the periodic table can now be used in NCs form [4]. Apart from the aforementioned applications, researchers are focusing on the development of small-scale gas sensors for applications ranging from dangerous gas detection to manufacturing process monitoring [5]. Nitrogen dioxide (NO_2) is a major air pollutant that can have substantial health and environmental consequences. This necessitates the development of gas sensing materials that can detect NO_2 quickly and recover promptly at low temperatures [6]. For decades, gas sensors have been used to detect harmful chemicals at various temperatures. Most researchers strive to create gas sensors that can operate at low concentrations and low temperatures, taking into account industry concerns about worker safety [1]. As liquefied petroleum gas (LPG) and other high-risk gases become more regularly used in industrial and home applications, the demand for high-performance and effective gas sensors with appropriate detecting materials has increased [5]. Because of their advantages and novel chemical and physical properties, metal oxides have attracted curiosity. Due to their excellent compatibility with microelectronics and low cost, metal oxide-based gas sensors have been widely investigated in this manner. Nanostructured semiconducting oxide materials like [1] TiO_2, $SrFe_{12}O_{19}$, hBN, CdS [6], ZnO, Fe_2O_3, WO_3, and SnO_2 are widely used as sensing materials to detect toxic and hazardous gases such as NH_3, CO_2, H_2S, H_2, ethanol, acetone, and NO_2 gases [1] due to their high sensitivity, quick response, easy availability, low cost, and good recovery. Metal oxide sensors have been discovered to be capable of

detecting hazardous gases, such as LPG and NO_2, at high temperatures, in terms of sensitivity, long-term stability, selectivity, and other factors [7]. Various methods for synthesising the above-mentioned sensing materials have been developed to date, including hydrothermal or solvothermal, reflux, precipitation, dip and spin coating, dc sputtering method, chemical method, and screen printing method [1].

1.1.1 Different Types of Nanoparticles

Nanoparticles can be classified based on their physical appearance and chemical properties. Semiconductor nanoparticles, carbon-based nanoparticles, ceramic nanoparticles, metal nanoparticles are such few examples.

1.2 Briefing of Smart Nanomaterials

1.2.1 Semiconductor Nanoparticles (i.e. Colloidal Quantum Dots)

Colloidal quantum dots (QDs) are semiconductor nanocrystals with a diameter of roughly 1–10 nm and hundreds to thousands of atoms [8–10]. Size-dependent electronic structure and photoluminescence (PL) emission from a phenomenon known as quantum confinement are two of the most distinguishing characteristics of QDs [8, 11]. For this chapter, semiconductor QD nanomaterials are divided into cadmium chalcogenides (group II–VI semiconductors), lead chalcogenides (group IV–VI semiconductors), non-heavy metal compounds (groups III–VI, I–III–VI, and I–VI semiconductors), silicon (group IV semiconductor), and cesium lead halide (groups I–IV–VII_3 semiconductors).

1.2.2 II – VI QDs

The first colloidal semiconductor material in which quantum confinement detected was CdS nanocrystals [12, 13]. Cadmium chalcogenide (CdX, X = S, Se, Te) semiconductors are still the most frequently utilised QD materials, as can be seen in Fig. 1.1a [14], and they continue to set the standard for PL**.** Similarly, the thought of extending the optical characteristic of NCs into the red and near-infrared ranges spurred the creation of mercury chalcogenide (HgX, X = S, Se, and Te) NCs [15]. The use of HgX NCs as broadband optical amplifiers in the telecommunication spectrum at wavelengths between 1.3 and 1.5 μm was the first use of HgX NCs. In the early 2000s, HgTe NCs were first employed in the telecom industry

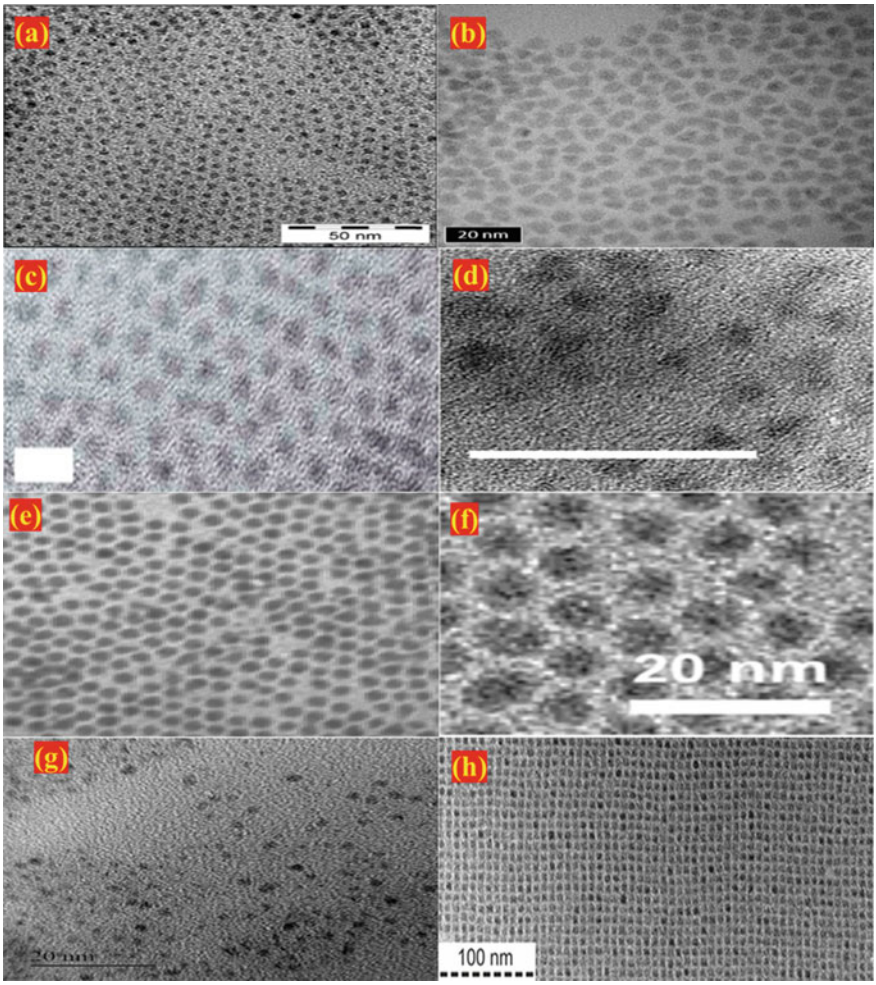

Fig. 1.1 **a** TEM image of spherical particles having a mean diameter of 4.88 ± 0.19 nm. There was no size selection made. The scale bar measures 50 nm. Adapted with permission from ref [14]. Copyright 2020 American Chemical Society. **b** Angular nanoparticles of 5.5 nm may be seen in this HR-TEM image. Here, 20 nm is the scale bar. Reprinted with permission from Ref. [22]. Copyright 2014 American Chemical Society. **c** PbS QDs TEM picture. The scale bar measures 10 nm. Reprinted with permission from Ref. [32]. Copyright 2021 American Chemical Society. **d** Images of InP QDs taken using a TEM (scale bar 20 nm). Adapted with permission from Ref. [2]. Copyright 2015 American Chemical Society. **e** $CuInS_2$ QDs TEM image (scale bar 50 nm). Adapted with the permission from ref [42]. Copyright 2009 American Chemical Society. **f** Ag_2S QDs TEM picture, scale bar 20 nm. Reprinted with the permission from ref [43]. Copyright 2014 American Chemical Society. **g** Si QDs TEM images with a 20 nm scale bar. Reproduced from Ref. [44]. Copyright 2019 American Chemical Society. **h** TEM photographs of $CsPbBr_3$ NCs with an edge length of 10.0 nm. Reprinted with the permission from Ref. [47]. Copyright 2019 American Chemical Society

[16]. NCs provide greater design flexibility for IR emitting devices since they are continuously spectrally adjustable. Mercury chalcogenides are II–VI semiconductors, making them ideal candidates for enhancing the optical properties of cadmium chalcogenide nanocrystals, the most studied material in colloidal nanocrystal form. The transition from Cd to Hg is related to an increased number of electrons and a lowered bandgap since mercury is placed below cadmium in the periodic table. As a result, mercury chalcogenides are a suitable candidate for infrared applications. In contrast to cadmium chalcogenides, HgTe has sparked a lot of interest among mercury chalcogenides [17], because CdTe is easier to oxidise, making it more difficult to produce and analyse than CdSe or CdS. HgTe colloidal growth has reached a mature stage, with size tunability (from a few nanometres to micrometres) [18], strong monodispersity, and shape control [19–21] as presented in Fig. 1.1b [22].

1.2.3 IV–VI QDs

Lead chalcogenide (i.e. PbX, X = S, Se, and Te) QDs, like cadmium chalcogenide QDs, are narrow-bandgap semiconductors with NIR emission that may be regulated by changing the nanocrystal size [23, 24]. Although the NIR emission of PbX materials is of potential relevance for biological imaging [23–25], it is also of importance for optoelectronic devices [26–28]. A TEM picture of PbS QDs [29–31] is shown in Fig. 1.1c [32].

1.2.4 III–V QDs

InP, InAs, GaP, and GaAs QDs are examples of type III–V QDs. Since its first colloidal production [33], InP QDs have been the most investigated of these materials and have piqued attention for chemical and biological investigation and imaging. InP QDs are a potential replacement for CdX QDs, with the added benefit of not containing heavy metals [32, 34–38] and addressed in the TEM picture [39–41] in Fig. 1.1d [2].

1.2.5 I–III–VI QDs

I–III–VI semiconductor QD materials are of interest as alternatives to CdX and PbX, similar to InP QDs. $CuInS_2$ (CIS), $CuInSe_2$ (CISe), and $AgInS_2$ (AIS) QDs are examples of I-III-VI semiconductor QDs, with CIS QDs being the most investigated. A TEM picture of CIS QDs [32, 41] is shown in Fig. 1.1e [42].

1.2.6 I–VI QDs

The most well-known I–VI semiconductor QDs are Ag_2S, Ag_2Se, and Ag_2Te QDs, with Ag_2S and Ag_2Se QDs being of particular relevance for biological applications [14]. TEM images of Ag_2S QDs are shown in Fig. 1.1f [43].

1.2.7 IV QDs

Silicon quantum dots (Si QDs) are more commonly referred to as silicon nanocrystals (Si NCs) and with good cause. A TEM picture of Si QDs is shown in Fig. 1.1g [44]. Germanium nanocrystals (Ge NCs) are similar to silicon nanocrystals (Si NCs) in many ways [32], but they are less developed and used [45].

1.2.8 Metal Halides Perovskite (I–IV-VII_3)-based Colloidal Quantum Dots

All-inorganic halide perovskites (i.e. $CsPbX_3$, X = Cl, Br, I, and mixed halide ions; [46]) are the potential semiconducting metal halides in the form of colloidal nanocrystals (NCs). Figure 1.1h [47] of $CsPbBr_3$ NCs with an edge length of 10.0 nm [46, 48, 49] shows a clear colloidal synthesis of monodisperse, 4–15 nm $CsPbX_3$ NCs with a cubic shape and cubic perovskite crystal structure. Because of the exciton Bohr diameter of up to 12 nm, $CsPbX_3$ NCs exhibit not only compositional bandgap engineering but also size tunability of their bandgap energies over the whole visible spectral range of 410–700 nm. Narrow emission line widths of 12–42 nm, significant quantum yields of 50–90%, and short radiative lifetimes of 1–29 ns characterise $CsPbX_3$ NCs' photoluminescence (PL) [46, 48, 49].

1.2.9 Carbon-Based Nanoparticles

Carbon nanoparticles come in a variety of forms. The smallest colloidal carbon allotrope materials discussed in this chapter include carbon nanotubes (CNTs), graphene-derived materials, carbon (quantum) dots, and nanodiamonds and will discuss briefly further in the next passages [32].

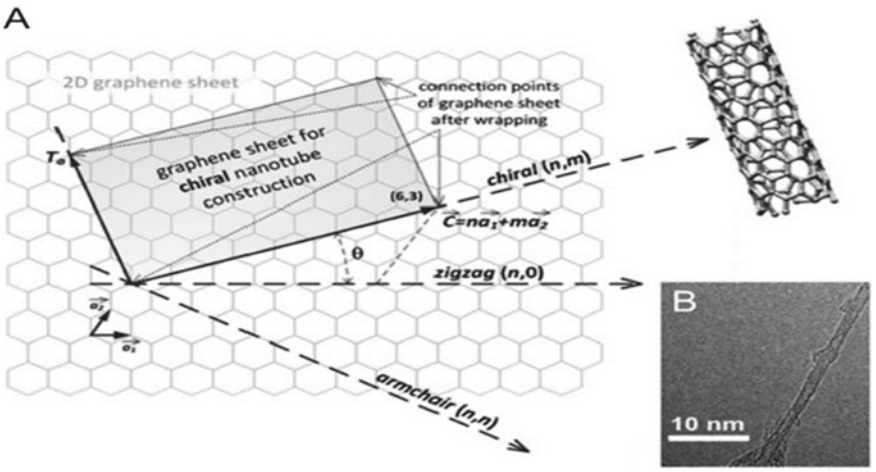

Fig. 1.2 SWCNTs. **a** Graphene being rolled up into SWCNTs in this illustration. Reprinted with permission from ref [32]. Copyright 2021 American chemical society. **b** SWCNT TEM picture. Adapted from Ref. [32]. Copyright 2021 the American chemical society

1.2.9.1 Carbon Nanotubes

Single-walled carbon nanotubes (SWCNTs) are quasi-one-dimensional materials made by rolling a piece of graphene sheet into a tube. SWCNTs are typically between 0.4 and 2 nm in diameter (but can be up to 7 nm) and come in a wide variety of lengths (from nanometers to micrometres) [32]. The chirality of the SWCNT is determined by the direction in which the graphene is rolled up, as shown in Fig. 1.2a [32], and is indicated by either two vectors (n, m) in the plane of its hexagonal lattice or, equivalently, the combination of the roll-up angle (0°–30°) and the nanotube diameter [32]. The chirality of a SWCNT dictates whether it is metallic ($n - m = 0$), semi-metallic ($n - m = 3p$, where p is an integer), or semiconducting ($n - m \neq 3p$). Multiwalled carbon nanotubes (MWCNTs) are concentrically nested SWCNTs with an interwall spacing of roughly 0.34 nm (comparable to the graphite interplane distance) and sizes varying from a few to many tens of nanometres [32]. A TEM picture of an SWCNT is shown in Fig. 1.2b [32].

1.2.9.2 Graphene-Derived Materials

A pristine graphene sheet is a quasi-infinite domain of sp^2 carbon with a zero-energy bandgap [32]. To allow for PL [32], the sp^2 domain must be made finite. Exfoliation of graphite into individual sheets of graphene oxide (GO) rich in oxygen-comprising functional groups is achieved using these many reported methods. The introduction of sp^3 carbon is the most major structural consequence of oxidation. The once quasi-infinite sp^2 carbon domain of graphene has been reduced to a set of discrete sp_2

domains (i.e. sp^2 islands delineated by regions of sp^3 carbons). Reduced graphene oxide (rGO) and its slightly reduced sibling, graphene oxide (GO), are both partially oxidised graphene compounds.

The difference is that GO is made by oxidising graphite, whereas rGO is made by reducing GO [32]. The reduction step's purpose is to minimise the number of oxygen-containing functional groups in the material while also restoring more and/or larger sp^2 domains. As a result, the changes in attributes between GO and rGO are due to variances in oxygen content. Top-down-prepared GO has lateral dimensions ranging from 100 nm to 1 m [32]. When these materials are processed into even smaller disc- or flake-shaped pieces (with a lateral dimension of 20 nm and three or fewer layers stacked, a height of 1 nm), the product is known as a graphene quantum dot (GQD) [32] and is shown in Fig. 1.3 [32].

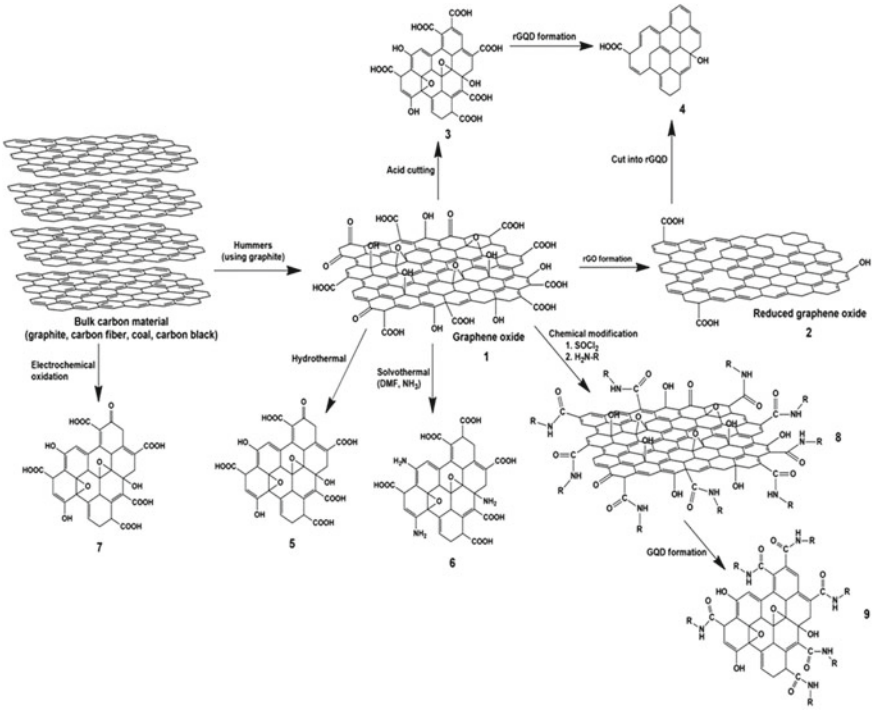

Fig. 1.3 Materials derived from graphene. GO, rGO, and GQD chemical representations and paths to these compounds starting with graphitic carbon. Reissued with permission from ref [32]. Copyright 2021 the American chemical society

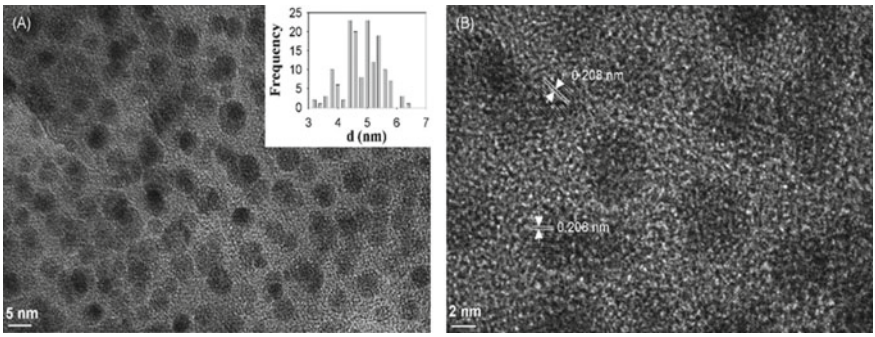

Fig. 1.4 Carbon nanoparticles in TEM micrographs with **a** Low resolution [50] and **b** High resolution. In A, the scale bar is 5 nm, while in B, it is 2 nm. The particle size histogram is shown in the inset of panel A. In panel B, the crystalline lattices are identified. Reprinted with the permission from ref [50]. Copyright 2009 American Chemical Society

1.2.9.3 Carbon Dots

Carbon dots (CDs) and carbon quantum dots (CQDs) are quasi-spherical with diameters of less than 10 nm [32]. Figure 1.4a [50] depicts a typical TEM image of carbon nanoparticles. The particles are mainly spherical and distributed equally across the TEM grid surface, as can be observed. The particle size dispersion is minimal, as seen in the size histogram in the figure inset, with the majority of the particles falling between 4.4 and 5.4 nm in diameter. The average diameter was found to be 4.80 ± 0.6 nm after statistical analysis of hundreds of carbon nanoparticles. High-resolution TEM examinations were used to determine the crystalline nature of the carbon particles. Figure 1.4b [50] shows a representative HR-TEM micrograph [32, 50].

1.2.9.4 Nanodiamonds

Nanodiamonds (NDs) are NPs with a diamond-like sp^3 carbon core that accounts for the majority of the carbon content [32]. NDs surfaces must always terminate in functional groups, and this core is sometimes surrounded by amorphous or graphitic layers of sp^2-rich carbon [32]. NDs can be of two types, for instance, detonation nanodiamonds (i.e. D-NDs) and high-pressure and high-temperature nanodiamonds (i.e. HPHT-NDs). The particles in D-ND synthesis have a relatively limited size distribution of roughly 35 nm and a round morphology, and they may make up a minority or a majority of the various carbon products produced by detonation [32]. Examples of TEM images of D-NDs and HPHT-NDs are shown in Fig. 1.5 [32]. HPHT-ND batches frequently have irregular shapes with sharp edges, broad size distributions, achievable average sizes ranging from 4 nm to tens or even hundreds of nanometres, and much less sp^2 carbon [32].

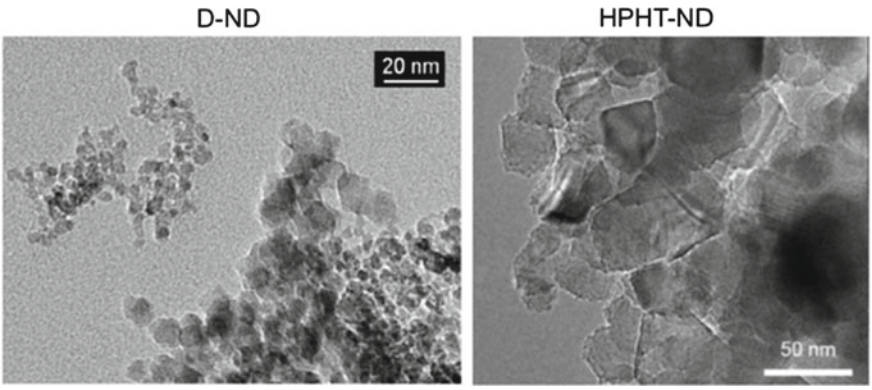

Fig. 1.5 NDs. D-NDs and HPHT-NDs TEM pictures. The D-ND image and the HPHT-ND image are from Ref. [32]. Copyright 2021 the American chemical society

1.3 Ceramic Nanoparticles

Ceramic nanoparticles have evolved as a novel class of nanoparticles that are extremely resistant to environmental changes [51]. Inorganic substances such as silica or alumina make up ceramic nanoparticles. Metals, metal oxides, and metal sulphides can all be employed to make nano-systems with different sizes, shapes, and porosities [32, 51]. Because of their favourable interactions with human tissues, ceramics such as calcium phosphates, silica, alumina, zirconium, iron oxides, carbonates, and titanium dioxide are used in a variety of medicinal applications [32, 51].

1.4 Metal Nanoparticles

Metal nanomaterials creation is one of the most ground-breaking fields in current nanoscience history, and significant efforts have been made to investigate the controlled synthesis of several types of metal nanostructures, such as silver, platinum, palladium, iron, cobalt, nickel, copper, and many other metals such as magnesium, aluminium, indium, germanium, cadmium, lead, and other low-melting point metals such as zinc, gallium, and tin, as well as their fascinating properties [52] and displayed in Fig. 1.6a [53] and Fig. 1.6b [54] of various sizes and shapes.

1.5 Briefing of Sensing Devices (i.e. Sensors)

A sensor, by definition, is a device that detects an external stimulus and replies with an electrical output [55, 56].

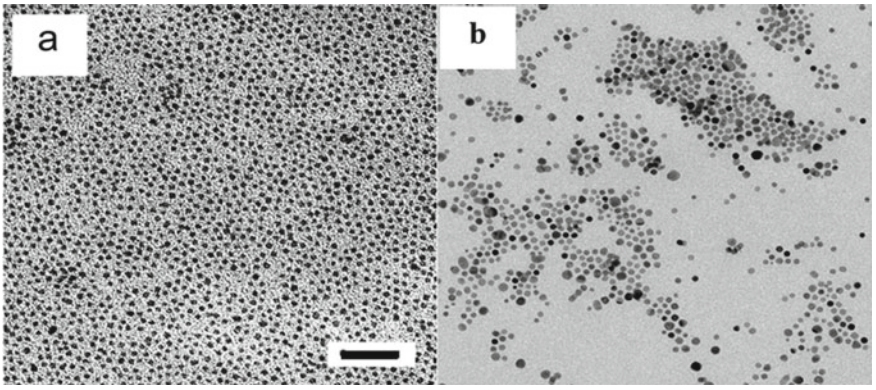

Fig. 1.6 **a** Au NPs TEM pictures. The scale bar is 20 nm long. Reissued with permission from Ref. [53]. Copyright 2009 American Chemical Society. **b** Ag NPs. TEM images 100 nm is the length of the scale bar. Reproduced with the permission from Ref. [54]. Copyright 2009 American Chemical Society

1.5.1 Different Types of Sensors

Temperature sensors, touch sensors, position sensors, light sensors, sound sensors, proximity sensors, accelerometer sensors, infrared sensors, pressure sensors, ultrasonic sensors, humidity sensors, colour sensors, chemical sensors, optical sensors, electrochemical sensors, seismic sensors, magnetic sensors, and gas sensors are all examples of sensors with different sensing targets or measurement principles. We have briefly discussed all these sensing devices but focused heavily on the gas sensor in this book chapter [55, 56].

1.5.1.1 Temperature Sensor

A temperature sensor is a piece of equipment that turns temperature into an electrical signal. Temperature sensors come in two varieties [55, 56].

(1) Contact temperature sensor; (2) noncontact temperature sensor.

- **Contact Temperature Sensor**

When these sensors come into contact with an object, they measure the temperature and send an electrical signal. The four basic types of contact temperature sensors are thermocouples, thermistors, resistive temperature detectors (i.e. RTD), and thermostats [55, 56].

- **Noncontact Temperature Sensor**

Instead of making direct touch with the object, these temperature metres use the heat source's radiation to measure the degree of hotness or coolness [55, 56].

1.5.1.2 Touch Sensor

Even if a human body touches anything, the surface information is immediately transmitted to the brain via the senses. Animals and plants can sense touch as well. As a result, the same technique can be applied to modern electronics [55, 56]. A sensor-related touch device is also being developed. We are increasingly seeing user interfaces that can be operated with a single touch. This criterion for sensing is employed in a variety of applications. Mobile phones, display screens, control panels, and other devices use touch sensors [55, 56].

- **Types of Touch Sensors**

Capacitive and resistive touch sensors are the two types of touch sensors [55, 56].

- **Touch Sensor Applications**

Capacitive touch sensors may be easily created with a pleasing appearance and for a lower cost. As a result, they are commonly used in mobile phones, iPods, and a variety of industrial and automotive applications. These sensors are used to measure distance, pressure, and other variables. Resistive touch sensors are another form of a touch sensor. It is unaffected by minor tactile sensations or contact [55, 56]. To start working requires a specific level of force. As a result, this sort of sensor is used in musical instrument keypads, resistive touchpads, and other applications. The most typical application of touch sensors is in water taps, where the volume of running water can be adjusted with a single touch [55, 56].

1.5.1.3 Position Sensors

The position sensor detects the distance between an object and a fixed point or position, either linearly or in rotation. Position can be determined by measuring the distance between two points moving away from fixed positions [55, 56]. A linear sensor can measure position displacement in a straight line, and rotational sensors can measure angular displacement. Position sensors, commonly known as potentiometers, are devices that measure an object's displacement [55, 56]. A potentiometer can be either an electrical or a resistive sensor since its operating principle is based on a change in wire resistance with length. This gadget transforms rotary or linear motion into electrical voltage [55, 56].

1.5.1.4 Light Sensors

A photoelectric passive sensor that converts light energy into an electrical signal output is known as a light sensor. It measures the ambient light, which includes light coming in from the outside, light coming in from within the room, and reflected light. The light-dependent resistor (LDR) or photoresistor is the most critical component

of a light sensor [55, 56]. It is a light-dependent resistor that changes resistance in response to the amount of light it receives. Lux is a unit of measurement for the amount of light falling on an LDR [55, 56].

1.5.1.5 Sound Sensor

The volume of sound is detected using a sound sensor, also called an auditory sensor. The acoustic wave is converted into an electrical signal by this device. These sensors can also detect non-audible sound pressure waves, making them helpful in a variety of situations. The majority of sound sensors are employed for security purposes [55, 56].

1.5.1.6 Proximity Sensor

A proximity sensor may detect the presence of an object nearby without any physical touch. It creates an electromagnetic field for an infrared electromagnetic radiation beam, and changes in the field provide a signal [55, 56]. The target of the proximity sensor is often referred to as the thing being felt [55, 56]. A proximity sensor has a high level of reliability because it has no mechanical parts and has no physical touch with the target [55, 56]. When used as a touch switch, it has a relatively short range. It is widely employed in industrial settings, such as food preparation, mobile phones [55, 56].

1.5.1.7 Accelerometer

The acceleration of an item is measured with this sensor. It works by detecting the acceleration of gravity and estimating the direction of the object [55, 56]. This sensor is a silicon-integrated circuit-based microelectromechanical system (MEMS) [55, 56]. Mechanical motion in an accelerometer is converted into an electrical signal using piezoelectric, piezoresistive, and capacitive components in these sensors [55, 56].

1.5.1.8 Infrared Sensor

The R_X (receiver) and T_X (transmitter) packets make up an infrared (IR) sensor (transmitter) [55, 56]. The infrared spectrum is transmitted by transmitters, while the IR spectrum range is received by receivers. The voltage is applied between its terminals in the IR spectrum, and it then emits rays [55, 56]. The primary premise of an IR sensor's operation is object reflectivity. When an object is positioned in front of the transmitter, the rays from the IR sensor tend to be reflected in the IR sensor [55, 56]. When a ray reflected by an object is received by the receiver, a voltage level is

generated across the terminal. The intensity of light reflected by the item determines the voltage level [55, 56]. The IR transmitter sends a signal within a specific range and to a specific distance, which is received by the IR receiver. When IR rays collide with a coloured surface, some of them are reflected. The brighter the colour, the more IR rays are reflected; conversely, the darker the surface, the more IR rays are absorbed by it and fewer IR rays are reflected [55, 56].

1.5.1.9 Pressure Sensor

This pressure is monitored using a pressure sensor, also known as a pressure transmitter because it converts pressure into an electrical signal [55, 56]. The strain gauge-based pressure sensor is the most popular type of pressure sensor. The atmospheric pressure causes a change in voltage. Fluid or gas flow, speed, water level, and altitude are among variables that can be measured with a pressure sensor [55, 56].

1.5.1.10 Ultrasonic Sensors

The distance between two objects is detected and measured using ultrasonic waves using an ultrasonic sensor [55, 56]. When a 40 kHz frequency wave is sent into the air by a transmitter, it is reflected and returned to the sensor when it is hindered by an object [55, 56]. These reflected waves are absorbed by the sensor's receiver. The sensor's output thus indicates the complete time ultrasonic waves take to travel from the transmitter to the item and back to the sensor's receiver [55]. Ultrasonic sensors are utilised in a variety of applications, including robotics, driverless cars, distance measurement, and radar systems [55, 56].

1.5.1.11 Humidity Sensor

A hygrometer is a gadget that directly measures humidity [55, 56]. Humidity refers to the amount of water in the air. Humidity is a non-electrical quantity that can be converted to an electrical quantity by applying resistance, capacitance, and impedance qualities [55, 56]. Humidity affects several aspects [55, 56]. Resistive hygrometers, capacitive hygrometers, microwave refractometers, aluminium oxide hygrometers, and crystal hygrometers are the five fundamental types of humidity sensors [55, 56].

1.5.1.12 Colour Sensor

A colour sensor is utilised to detect and distinguish various colour patterns [55, 56]. Red, green, blue, and clear photodiodes make up the device (no colour). These photodiodes are connected in series and serve as filters [55, 56]. A red colour filter,

for example, can be used to detect red colour [55, 56]. Photodiodes detect colour light signals and generate square wave signals with a frequency proportional to light intensity, which are then transferred to the microcontroller, resulting in the colour output [55, 56].

1.5.1.13 Chemical Sensor

A chemical sensor captures chemical data from a chemical process and sends it to a computer [55, 56]. Chemical information can come in the form of composition, concentration, and chemical activity, and it can come through chemical reactions or physical activities [55, 56]. It has a variety of uses, including in-home appliances and the chemical industry [55, 56]. Optical and electrochemical chemical sensors are employed to detect the composition [55, 56].

Optical Sensor

An emitter and a detector are the two most important parts of an optical sensor. Light is detected by the emitter and sent to the optical sensor, where light rays strike the analyte and may be reflected or refracted [55, 56]. These reflected or refracted rays are passed through by the detector [55, 56]. The detector now receives these lights and, based on their intensity, determines which chemical molecule is present [55, 56].

Electrochemical Sensor

The electrochemical sensor operates by interacting with the molecules of interest in the gas and creating an electric signal proportional to the amount of compound present [55, 56]. It consists of electrodes and sensing modules separated by an electrolyte layer. The cathode is one plate, and the anode is the other. Certain ions from the solution absorb an external membrane that is injected into the solution [55, 56]. As a result, both the chemical and electromagnetic properties of the solution change; as a result, a shift in the electromagnetic field guarantees that the gas' chemical composition is preserved [55].

1.5.1.14 Seismic Sensor

A seismic sensor detects and records minor ground vibrations by measuring, amplifying, and recording them [55]. It is also known as a seismometer, and it is used to determine the precise specifics of earthquakes, volcanic eruptions, and other vibrations [55, 56]. Inertial seismometers and strain metres or extensometer seismic sensors are the two types of seismic sensors [55, 56].

1.5.1.15 Magnetic Sensor

Magnetic sensors give a proportional output when a magnetic field is present or disrupted, such as flux, strength, or direction. It converts magnetic information into an electrical signal that can be processed by an electronic circuit [55, 56]. A magnetic sensor's output rises in a high magnetic field and falls in a weak magnetic field [55].

1.5.1.16 Biosensor

A biosensor is an analytical device that converts a biological response into a signal that can be read and quantified. Biosensors can analyse body fluids, food samples, and cell cultures [57]. Immobilised biological recognition components on sensor substrates with a specific binding affinity for target molecules interact with the targets in such a way that the biosensor achieves high selectivity and sensitivity [57]. TiO_2, ZnO, NiO, and other semiconductor nanoparticles are attractive candidates for immobilising biological components because of these properties (e.g. low cost, high stability, and biocompatibility) [57]. Electrochemical transducers are widely employed in biosensing applications because of their functionalities, which are carried out utilising electrochemical techniques (e.g. amperometric and potentiometric process) [57]. Biochemical reactions are at the heart of biosensing, especially electrochemical biosensing [57]. A measurable current (amperometric), a detectable potential (potentiometric), or charge buildup are created when the conductive properties of a medium between electrodes change [57]. For this reason, enzyme, haemoglobin, antibody, antigen, cells, DNA, and bacteria corresponding to a given target are usually added to a semiconductor electrode [57]. In addition to gathering electrochemical signals, a light transducer could be used to power an optical biosensor [57]. Surface plasmon resonance (SPR), electrochemiluminescence (ECL), and fluorescence are three key ways by which biomolecules bond to targets that affect the optical characteristics of the electrode surface, allowing the variation of reflected or emitted light to be proportionate to the target concentration [57].

1.5.1.17 Gas Sensors

A gas sensor is a device that detects changes in the concentration of dangerous gases in order to maintain the system safe and avert any unexpected problems [55, 56, 58]. The sensor provides a agreeing potential difference based on the gas concentration by modifying the resistance of the substance inside the sensor, which may be accepted as output voltage [55, 56, 58]. The nature and concentration of the gas can be determined using this voltage value.

Various Kinds of Gas Sensors

There are various types of gas sensors available today, but **semiconductor metal oxide-based gas sensors** are the most common and commonly utilised; therefore, we will concentrate on them in this area of the book chapter [55, 56, 58].

Construction of Gas Sensors

A detecting element will be present in all gas sensors, and it will incorporate the components stated briefly below [55, 56, 58].

- **Gas Sensing Layer**

It is the sensor's principal component for detecting changes in gas concentration and adjusting the electrical resistance [56]. Tin dioxide (SnO_2) is used as the sensing element since it possesses extra electrons (donor element) [56]. When dangerous gases are identified, the resistance of the element and the current flowing through it vary, signalling an alteration in gas concentration [55, 56, 58].

- **Heater Coil**

The heating coil is designed to burn into the sensor element, improving sensitivity and efficiency. It is made of nickel–chromium, a metal with a high melting point that can withstand high temperatures without melting [55, 56, 58].

- **Electrode Line**

The effectiveness of transferring those small currents is especially significant because the detecting device makes such a little current when the gas is detected. As a result, platinum wires come into action, assisting in the efficient movement of electrons [55, 56, 58].

- **Electrode**

At this point, the sensor layer's output is linked to the electrode line. The output current must be able to reach the target terminal. Gold (i.e. Au) is used as an electrode because it is an excellent conductor [55, 56, 58].

- **Tubular Ceramic**

The heating coil and the gas sensing layer are separated by a tubular ceramic made of aluminium oxide (Al_2O_3). Its high melting point facilitates the preheating of the sensor layer, resulting in excellent sensitivity and efficient output current [55, 56, 58].

- **Mesh Over the Sensing Element**

A metal mesh is put over the sensing device and the setup to protect it from corrosive particles while also preventing dust particles from entering the mesh [55, 56, 58], as seen in Fig. 1.7a [58].

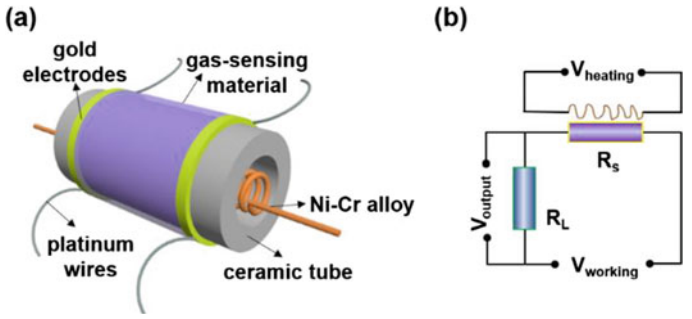

Fig. 1.7 **a** Side-heated gas sensor is depicted in diagrammatic form [58]. **b** Gas-detecting test electric circuit. Reprinted with the permission from Ref. [58]. Copyright 2021 Multidisciplinary Digital Publishing Institute

Sensor Measurement

The gas response of the as-fabricated gas sensors was determined utilising the intelligent gas sensing system after the gas sensor was successfully manufactured from SnO_2 samples. Figure 1.7b [58] depicts the electric circuit for gas sensing detection [58]. The as-fabricated gas sensor is connected in series with a load resistor (R_L) (i.e. the value of R_L could be anything between $10K\Omega$ and $47K\Omega$.) at a specific voltage $\left(V_{\text{Working}}\right)$. The gas sensor's resistance value (R_s) can be calculated using the load resistance's output voltage $\left(V_{\text{Output}}\right)$ [58]. The gas sensor's working temperature is automatically altered by varying the heating voltage $\left(V_{\text{Heating}}\right)$. When a target gas is introduced into the test chamber, the sensor resistance varies, as does the load resistor [58]. As a result, the gas response of the gas sensor can be characterised as follows:

$$\text{Gas Response } S = R_a / R_g \tag{1.1}$$

R_g signifies the gas sensor's resistance in target gas, whereas R_a denotes the gas sensor's resistance in the air [58], and Fig. 1.7b depicts the electric circuit.

Applications of Gas Sensors

- Used in businesses to detect harmful gas concentrations [55, 56, 58]
- Used in homes to detect a disaster
- Used on oil rigs to monitor the concentration of gases discharged
- In hotels, it is used to keep customers from smoking
- In offices, it is used to check the air quality
- Used to monitor CO_2 levels in air conditioners [55, 56, 58]
- It is used to find out if there is a fire
- Used in mines to monitor gas concentrations
- Analyser for breathing [56].

1.6 Modern Sensors

During the last decade, sensor technology has evolved substantially in terms of compactness, intelligence, and sensitivity [55]. Photosensors, optical sensors, capacitive sensors, and almost all sensors have been essentially supplanted by microelectromechanical systems (MEMS) [55]. Sensors are included in compact forms in all modern computing and navigation devices, which is why an average smartphone contains roughly 22 sensors for diverse functions [55, 56, 58]. Sensor technologies have progressed to the point that they are now sophisticated smart sensors that can be worn [55, 56, 58]. This can be seen in smartwatches, smart devices, and even large applications such as self-driving automobiles, which use hundreds of smart sensors to enable seamless and smooth driving without the need for a driver [55, 56, 58].

1.7 Conclusions

We covered a quick overview of nanomaterials (NMs) and several types of sensing devices in this book chapter. Nanomaterials have a promising future, but they must progress beyond being a novelty or a fad. The creation of applications (e.g. employed in sensing devices) that uniquely leverage the strengths and minimise the weaknesses of each material is critical to realising the potential of NMs. Protection amenities are quite important in today's hectic lifestyle. The need for sensing devices has skyrocketed in recent years. The uses, cost, precision, and range of these sensors are used to classify them. The many types of sensors accessible include thermal, electrical, magnetic optical, mechanical, and chemical sensors. Cognitive and smart sensors are currently used in all modern applications, thanks to advancements in sensor technology.

References

1. M.R. Waikar, P.M. Raste, R.K. Sonker, V. Gupta, M. Tomar, M.D. Shirsat, R.G. Sonkawade, Enhancement in NH_3 sensing performance of ZnO thin-film via gamma-irradiation. J. Alloy. Compd. **830**, 154641 (2020)
2. M.D. Tessier, D. Dupont, K.D. Nolf, J.D. Roo, Z. Hens, Economic and size-tunable synthesis of InP/ZnE (E= S, Se) colloidal quantum dots. Chem. Mater. **27**(13), 4893–4898 (2015)
3. D. Bera, L. Qian, T.-K. Tseng, P.H. Holloway, Quantum dots and their multimodal applications: a review. Materials **3**(4), 2260–2345 (2010)
4. C. Gréboval, A. Chu, N. Goubet, C. Livache, S. Ithurria, E. Lhuillier, Mercury chalcogenide quantum dots: material perspective for device integration. Chem. Rev. **121**(7), 3627–3700 (2021)
5. C. Gautam, C.S. Tiwary, L.D. Machado, S. Jose, S. Ozden, S. Biradar, D.S. Galvao, R.K. Sonker, B.C. Yadav, R. Vajtai, P.M. Ajayan, Synthesis and porous h-BN 3D architectures for effective humidity and gas sensors. RSC Adv. **6**(91), 87888–87896 (2016)

6. R.K. Sonker, B.C. Yadav, V. Gupta, M. Tomar, Synthesis of CdS nanoparticle by sol-gel method as low temperature NO_2 sensor. Mater. Chem. Phys. **239**, 121975 (2020)
7. R.K. Sonker, B.C. Yadav, V. Gupta, M. Tomar, Fabrication and characterization of ZnO-TiO2-PANI (ZTP) micro/nanoballs for the detection of flammable and toxic gases. J. Hazard. Mater. **370**, 126–137 (2019)
8. C.J. Murphy, J.L. Coffer, Quantum dots: a primer. Appl. Spectrosc. **56**(1), 16A-27A (2002)
9. E. Petryayeva, W. Russ Algar, I.L. Medintz, Quantum dots in bioanalysis: a review of applications across various platforms for fluorescence spectroscopy and imaging. Appl. Spectroscopy **67**(3), 215–252 (2013)
10. N. Hildebrandt, C.M. Spillmann, W. Russ Algar, T. Pons, M.H. Stewart, E. Oh, K. Susumu, S.A. Diaz, J.B. Delehanty, I.L. Medintz, Energy transfer with semiconductor quantum dot bioconjugates: a versatile platform for biosensing, energy harvesting, and other developing applications. Chem. Rev. **117**(2), 536–711 (2017)
11. W.R. Algar, K. Susumu, J.B. Delehanty, I.L. Medintz, Semiconductor quantum dots in bioanalysis: crossing the valley of death (2011), pp. 8826–8837
12. M. Sandroni, K. David Wegner, D. Aldakov, P. Reiss, Prospects of chalcopyrite-type nanocrystals for energy applications. ACS Energy Lett. **2**(5), 1076–1088 (2017)
13. Nanocrystals in their prime. Nat. Nanotechnol. **9**, 325–325 (2014). https://doi.org/10.1038/nnano.2014.101
14. F.S. Riehle, K. Yu, Role of alcohol in the synthesis of CdS quantum dots. Chem. Mater. **32**(4), 1430–1438 (2020)
15. A.L. Rogach, A. Eychmüller, S.G. Hickey, S.V. Kershaw, Infrared-emitting colloidal nanocrystals: synthesis, assembly, spectroscopy, and applications. Small **3**(4), 536–557 (2007)
16. A. Rogach, S.V. Kershaw, M. Burt, M.T. Harrison, A. Kornowski, A. Eychmüller, H. Weller, Colloidally prepared HgTe nanocrystals with strong room-temperature infrared luminescence. Adv. Mater. **11**(7), 552–555 (1999)
17. M. Green, H. Mirzai, Synthetic routes to mercury chalcogenide quantum dots. J. Mater. Chem. C **6**(19), 5097–5112 (2018)
18. N. Goubet, A. Jagtap, C. Livache, B. Martinez, H. Portalès, X. Zhen Xu, R.P.S.M. Lobo, B. Dubertret, E. Lhuillier, Terahertz HgTe nanocrystals: beyond confinement. J. Am. Chem. Soc. **140**(15), 5033–5036 (2018)
19. E. Izquierdo, A. Robin, S. Keuleyan, N. Lequeux, E. Lhuillier, S. Ithurria, Strongly confined HgTe 2D nanoplatelets as narrow near-infrared emitters. J. Am. Chem. Soc. **138**(33), 10496–10501 (2016)
20. G. Shen, M. Chen, P. Guyot-Sionnest, Synthesis of nonaggregating HgTe colloidal quantum dots and the emergence of air-stable n-doping. J. Phys. Chem. Lett. **8**(10), 2224–2228 (2017)
21. H. Zhang, P. Guyot-Sionnest, Shape-controlled HgTe colloidal quantum dots and reduced spin-orbit splitting in the tetrahedral shape. J. Phys. Chem. Lett. **11**(16), 6860–6866 (2020)
22. S.E. Keuleyan, P. Guyot-Sionnest, C. Delerue, G. Allan, Mercury telluride colloidal quantum dots: electronic structure, size-dependent spectra, and photocurrent detection up to 12 μm. ACS Nano **8**(8), 8676–8682 (2014)
23. J. Kim, D. Choi, K.S. Jeong, Self-doped colloidal semiconductor nanocrystals with intraband transitions in steady state. Chem. Commun. **54**(61), 8435–8445 (2018)
24. A. Jagtap, C. Livache, B. Martinez, J. Qu, A. Chu, C. Gréboval, N. Goubet, E. Lhuillier, Emergence of intraband transitions in colloidal nanocrystals. Opt. Mater. Express **8**(5), 1174–1183 (2018)
25. Y. Park, S. Jeong, S. Kim, Medically translatable quantum dots for biosensing and imaging. J. Photochem. Photobiol., C **30**, 51–70 (2017)
26. P. Zhao, Q. Xu, J. Tao, Z. Jin, Y. Pan, C. Yu, Z. Yu, Near infrared quantum dots in biomedical applications: current status and future perspective. Wiley Interdiscip. Rev. Nanomedicine Nanobiotechnol. **10**(3), e1483 (2018)
27. C.M. Evans, L.C. Cass, K.E. Knowles, D.B. Tice, R.P.H. Chang, E.A. Weiss, Review of the synthesis and properties of colloidal quantum dots: the evolving role of coordinating surface ligands. J. Coordination Chem. **65**(13), 2391–2414 (2012)

28. A. Shrestha, M. Batmunkh, A. Tricoli, S.Z. Qiao, S. Dai, Near-infrared active lead chalcogenide quantum dots: preparation, post-synthesis ligand exchange, and applications in solar cells. Angewandte Chemie Int. Ed. **58**(16), 5202–5224 (2019)
29. Y. Jang, A. Shapiro, M. Isarov, A. Rubin-Brusilovski, A. Safran, A.K. Budniak, F. Horani, J. Dehnel, A. Sashchiuk, E. Lifshitz, Interface control of electronic and optical properties in IV–VI and II–VI core/shell colloidal quantum dots: a review. Chem. Commun. **53**(6), 1002–1024 (2017)
30. H. Lu, G.M. Carroll, N.R. Neale, M.C. Beard, Infrared quantum dots: progress, challenges, and opportunities. ACS Nano **13**(2), 939–953 (2019)
31. A. Zebibula, N. Alifu, L. Xia, C. Sun, X. Yu, D. Xue, L. Liu, G. Li, J. Qian, Ultrastable and biocompatible NIR-II quantum dots for functional bioimaging. Adv. Functional Mater. **28**(9), 1703451 (2018)
32. W.R. Algar, M. Massey, K. Rees, R. Higgins, K.D. Krause, G.H. Darwish, W.J. Peveler, et al., Photoluminescent nanoparticles for chemical and biological analysis and imaging. Chem. Rev. **121**(15), 9243–9358 (2021)
33. H. Fu, S.-W. Tsang, Infrared colloidal lead chalcogenide nanocrystals: synthesis, properties, and photovoltaic applications. Nanoscale **4**(7), 2187–2201 (2012)
34. O.I. Micic, J.R. Sprague, C.J. Curtis, K.M. Jones, J.L. Machol, A.J. Nozik, H. Giessen, B. Fluegel, G. Mohs, N.J. Peyghambarian, Synthesis and characterization of InP, GaP, and GaInP2 quantum dots. J. Phys. Chem. **99**(19), 7754–7759 (1995)
35. G. Xu, S. Zeng, B. Zhang, M.T. Swihart, K.-T. Yong, P.N. Prasad, New generation cadmium-free quantum dots for biophotonics and nanomedicine. Chem. Rev. **116**(19), 12234–12327 (2016)
36. R.-S. Liu, ed., *Phosphors, up conversion nano particles, quantum dots and their applications*, Vol. 1 (Springer, Berlin, 2017). https://doi.org/10.1007/978-981-10-1590-8
37. Z. Ranjbar-Navazi, Y. Omidi, M. Eskandani, S. Davaran, Cadmium-free quantum dot-based theranostics. TrAC Trends Anal. Chem. **118**, 386–400 (2019)
38. V. Brunetti, H. Chibli, R. Fiammengo, A. Galeone, M.A. Malvindi, G. Vecchio, R. Cingolani, J.L. Nadeau, P.P. Pompa, InP/ZnS as a safer alternative to CdSe/ZnS core/shell quantum dots: in vitro and in vivo toxicity assessment. Nanoscale **5**(1), 307–317 (2013)
39. G. Lin, Q. Ouyang, R. Hu, Z. Ding, J. Tian, F. Yin, G. Xu, Q. Chen, X. Wang, K.-T. Yong, In vivo toxicity assessment of non-cadmium quantum dots in BALB/c mice. Nanomed. Nanotechnol. Biol. Med. **11**(2), 341–350 (2015)
40. A. Narayanaswamy, L.F. Feiner, P.J. Van Der Zaag, Temperature dependence of the photoluminescence of InP/ZnS quantum dots. J. Phys. Chem. C **112**(17), 6775–6780 (2008)
41. O.T. Bruns, T.S. Bischof, D.K. Harris, D. Franke, Y. Shi, L. Riedemann, A. Bartelt, et al., Next-generation in vivo optical imaging with short-wave infrared quantum dots. Nat. Biomed. Eng. **1**(4), 1–11 (2017)
42. R. Xie, M. Rutherford, X. Peng, Formation of high-quality I− III− VI semiconductor nanocrystals by tuning relative reactivity of cationic precursors. J. Am. Chem. Soc. **131**(15), 5691–5697 (2009)
43. Y. Zhang, Y. Liu, C. Li, X. Chen, Q. Wang, Controlled synthesis of Ag_2S quantum dots and experimental determination of the exciton Bohr radius. J. Phys. Chem. C **118**(9), 4918–4923 (2014)
44. B. Sharma, S. Tanwar, T. Sen, One pot green synthesis of Si quantum dots and catalytic Au nanoparticle–Si quantum dot nanocomposite. ACS Sustain. Chem. Eng. **7**(3), 3309–3318 (2019)
45. R. Gui, H. Jin, Z. Wang, L. Tan, Recent advances in synthetic methods and applications of colloidal silver chalcogenide quantum dots. Coord. Chem. Rev. **296**, 91–124 (2015)
46. V. Kumar, V. Nagal, R. Kumar, S. Srivastava, B.K. Gupta, M. Kumar, A.K. Hafiz, K. Singh, Influence of the rate of radiation energy on the charge-carrier kinetics application of all-inorganic CsPbBr 3 perovskite nanocrystals. RSC Adv. **10**(57), 34651–34657 (2020)
47. S.T. Ochsenbein, F. Krieg, Y. Shynkarenko, G. Rainò, M.V. Kovalenko, Engineering color-stable blue light-emitting diodes with lead halide perovskite nanocrystals. ACS Appl. Mater. Interfaces **11**(24), 21655–21660 (2019)

48. V. Kumar, V. Nagal, S. Srivastava, M. Kumar, B.K. Gupta, A.K. Hafiz, K. Singh, Power dependent hot carrier cooling dynamics in trioctylphosphine capped CsPbBr 3 perovskite quantum dots using ultrafast spectroscopy. ChemistrySelect **6**(38), 10165–10177 (2021)
49. V. Nagal, V. Kumar, R. Kumar, K. Singh, A. Khosla, R. Ahmad, A. Khurram Hafiz, CsPbBr3 nanoplatelets: synthesis and understanding of ultraviolet light-induced structural phase change and luminescence degradation. ECS J. Solid State Sci. Technol. **10**(9), 096002 (2021)
50. L. Tian, D. Ghosh, W. Chen, S. Pradhan, X. Chang, S. Chen, Nanosized carbon particles from natural gas soot. Chem. Mater. **21**(13), 2803–2809 (2009)
51. G.S. Armatas, M.G. Kanatzidis, Mesostructured germanium with cubic pore symmetry. Nature **441**(7097), 1122–1125 (2006)
52. C.N.R. Rao, H.S.S. Ramakrishna Matte, R. Voggu, A. Govindaraj, Recent progress in the synthesis of inorganic nanoparticles. Dalton Trans. **41**(17), 5089–5120 (2012)
53. M. Kanehara, J.-I. Sakurai, H. Sugimura, T. Teranishi, Room-temperature size evolution of thiol-protected gold nanoparticles assisted by proton acids and halogen anions. J. Am. Chem. Soc. **131**(5), 1630–1631 (2009)
54. Q. Zhang, C. Cobley, L. Au, M. McKiernan, A. Schwartz, L.-P. Wen, J. Chen, Y. Xia, Production of Ag nanocubes on a scale of 0.1 g per batch by protecting the NaHS-mediated polyol synthesis with argon. ACS Appl. Mater. Interfaces **1**(9), 2044–2048 (2009)
55. G.R. Sinha, *Advances in Modern Sensors; Physics, Design, Simulation and Applications* (2020). https://doi.org/10.1088/978-0-7503-2707-7
56. M.J. McGrath, C. Ni Scanaill, *Sensor Technologies: Healthcare, Wellness, and Environmental Applications* (Springer Nature, 2013). https://doi.org/10.1007/978-1-4302-6014-1
57. J. Bai, B. Zhou, Titanium dioxide nanomaterials for sensor applications. Chem. Rev. **114**(19), 10131–10176 (2014)
58. P. Ren, Q. Shi, L. Qi, A gas sensor based on network nanowire for H_2S monitor in construction waste landfill. Chemosensors **9**(7), 156 (2021). https://doi.org/10.3390/chemosensors9070156